Middle Tertiary plutonism in the Santa Catalina and Tortolita Mountains, Arizona

By

S. C. Creasey, Norman G. Banks, R. P. Ashley, and Ted G. Theodore
U.S. Geological Survey, Menlo Park, California 94025

U.S. Geological Survey
Open-file Report 76-262
1976

This report is preliminary and has not been edited or reviewed for conformity with Geological Survey standards and nomenclature.

CONTENTS

	Page
Abstract	1
Introduction	1
General geology	2
Radiometric ages	5
Epilogue	15
References cited	16

ILLUSTRATIONS

Page

Figure 1. Geologic sketch map of the Santa Catalina Mountains -- 3

2. Locations of samples listed in tables 1, 2, and 3. Stipple pattern indicates the outcrop areas of the quartz monzonite of Samaniego Ridge ---------- 7

3. Bar graphs of new fission-track and K-Ar ages of the quartz monzonite of Samaniego Ridge and the quartz monzonite of the Tortolita Mountains, Santa Catalina and Tortolita Mountains ---------- 11

4. Bar graphs of published K-Ar ages of quartz monzonite of Samaniego Ridge and gneissic rocks, Santa Catalina and Tortolita Mountains ---------- 13

TABLES

Table 1. New fission-track and K-Ar ages of the quartz monzonite of Samaniego Ridge and the quartz monzonite of the Tortolita Mountains, from the Santa Catalina and Tortolita Mountains ---------- 6

2. Previously published K-Ar ages of the quartz monzonite of Samaniego Ridge, Oracle Granite, and gneissic rocks, Santa Catalina and Tortolita Mountains ---------- 8

3. Previously published Rb-Sr ages of the quartz monzonite of Samaniego Ridge, Oracle Granite, and gneissic rocks, Santa Catalina Mountains ---------- 14

4. Chemical, spectrographic, normative, and modal analyses of rocks from the Santa Catalina and Tortolita Mountains ---------- 18

Analytical data for fission-track ages for Santa Catalina and Tortolita Mountains ---------- 19

Analytical data for K-Ar ages for the Santa Catalina and Tortolita Mountains ---------- 20

ABSTRACT

Recent reconnaissance geologic mapping in the Santa Catalina and Tortolita Mountains of southeastern Arizona, supplemented by new and published potassium-argon and fission-track ages, suggests that a large middle Tertiary (about 25 m.y.) composite batholith crops out extensively in both mountains. More than two-thirds of the batholith and the contiguous wallrocks are gneissic, the gneissosity comprising strong cataclasis and mylonitization, penetrative planar and linear structures, and crystallization of muscovite and biotite in the foliation planes. New radiometric ages indicate the deformation followed the crystallization of the batholith so closely that the K-Ar dating method cannot distinguish a difference, whereas previously published ages from the gneisses indicate a short time interval between the two events.

INTRODUCTION

The authors recently mapped the geology of the Santa Catalina and a small part of the Tortolita Mountains in reconnaissance (Banks, 1976; Creasey and Theodore, 1975), and made 26 new radiometric age determinations to help interpret the plutonic and structural history of the region. A synopsis of the geology of the Santa Catalina Mountains, which includes some heretofore unpublished geology of the northern flank of the mountains, is shown on figure 1.

The Santa Catalina Mountains were mapped twice by the U.S. Geological Survey previous to our work, but neither of the earlier maps were published. The first map was made by C. F. Tolman, Jr., at a scale of 1:125,000 in 1911-12. He also prepared a report in 1914, but neither map nor report was published. In 1930, B. N. Moore of the U.S. Geological Survey was assigned to update the report for publication. In 1938, he submitted a report, but before the report was approved for publication, he left the Geological Survey, and again the report was never published. However, a summary of Moore's report, prepared by B. S. Butler and R. M. Hernon, and a black-and-white version of the map were released in open file (Moore and others, 1949). In addition, many maps from theses by students from the University of Arizona cover separate parts of the Santa Catalina. Except for a mid-Tertiary rather than a Late Cretaceous or early Tertiary age for emplacement of the batholith and development of the gneiss, our interpretations do not differ substantially from those of B. N. Moore.

New K-Ar and fission-track ages are listed in table 1, and to permit comparison, previously published K-Ar and Rb-Sr ages of rocks in the Santa Catalina Mountains are listed on tables 2 and 3. These data are summarized by the bar graphs of figures 3 and 4. Chemical and spectrographic analyses, modes, and norms of our dated rocks and two additional samples are listed at the end of the report (table 4). The

locations of all samples, including ours and those available for dated samples reported in the literature are indicated on figure 2. The analytical data supporting the radiometric ages are tabulated at the end of the report.

GENERAL GEOLOGY

The Santa Catalina Mountains are one of the structurally and lithologically complex mountains of the Basin and Range province in southeastern Arizona (fig. 1). At the northern end of the Santa Catalina, the Mogul fault is the dominant structure. North of the Mogul fault, only Oracle Granite, locally cut by dikes and quartz veins, crops out, whereas south of the fault and along the northeastern flank, the range consists of Precambrian, Paleozoic, and Mesozoic sedimentary rocks, all intruded by quartz diorite, quartz monzonite, and granodiorite porphyry.

The central core of the Santa Catalina Mountains consists of a large composite batholith of middle Tertiary age. Apparently the batholith extends to the northwest into the Tortolita Mountains, where it has been partly mapped in reconnaissance by the authors, and to the southeast into the Rincon Mountains. The batholith comprises at least two intrusive phases hereafter referred to as the quartz monzonite of Samaniego Ridge and the quartz monzonite of the Tortolita Mountains. Except for two dikes of the quartz monzonite of the Tortolita Mountains, just east of the Pirate fault, only the quartz monzonite of Samaniego Ridge crops out in the Santa Catalina Mountains. The main mass of the quartz monzonite of the Tortolita Mountains lies to the west of figure 1 in the Tortolita Mountains.

The southwestern flank of the Santa Catalina consists of a mixture of quartz monzonite of Samaniego Ridge and roof pendants, principally of Oracle Granite, but also of granodiorite and Precambrian rocks. The quartz monzonite forms a sill-like body more than 2 km thick which intruded the contact between the Apache Group composed of sedimentary rocks lying to the north and the Oracle Granite on the south.

Roof pendants and xenoliths of Apache Group, Pinal Schist, Paleozoic and Mesozoic sedimentary rocks, and quartz diorite (Leatherwood) occur here and there in the quartz monzonite. They are common near Mount Lemmon, which is the highest peak in the Santa Catalina.

Emplacement of the batholith was essentially coeval with the development of extensive penetrative planar and linear structures that characterize the gneisses forming the southeastern forerange of the Santa Catalina Mountains and extending both northwestward into the Tortolita Mountains and southeastward into the Rincon Mountains, which join the Santa Catalina Mountains along a low divide known locally as the Redington Pass. The contact between gneissic and nongneissic parts

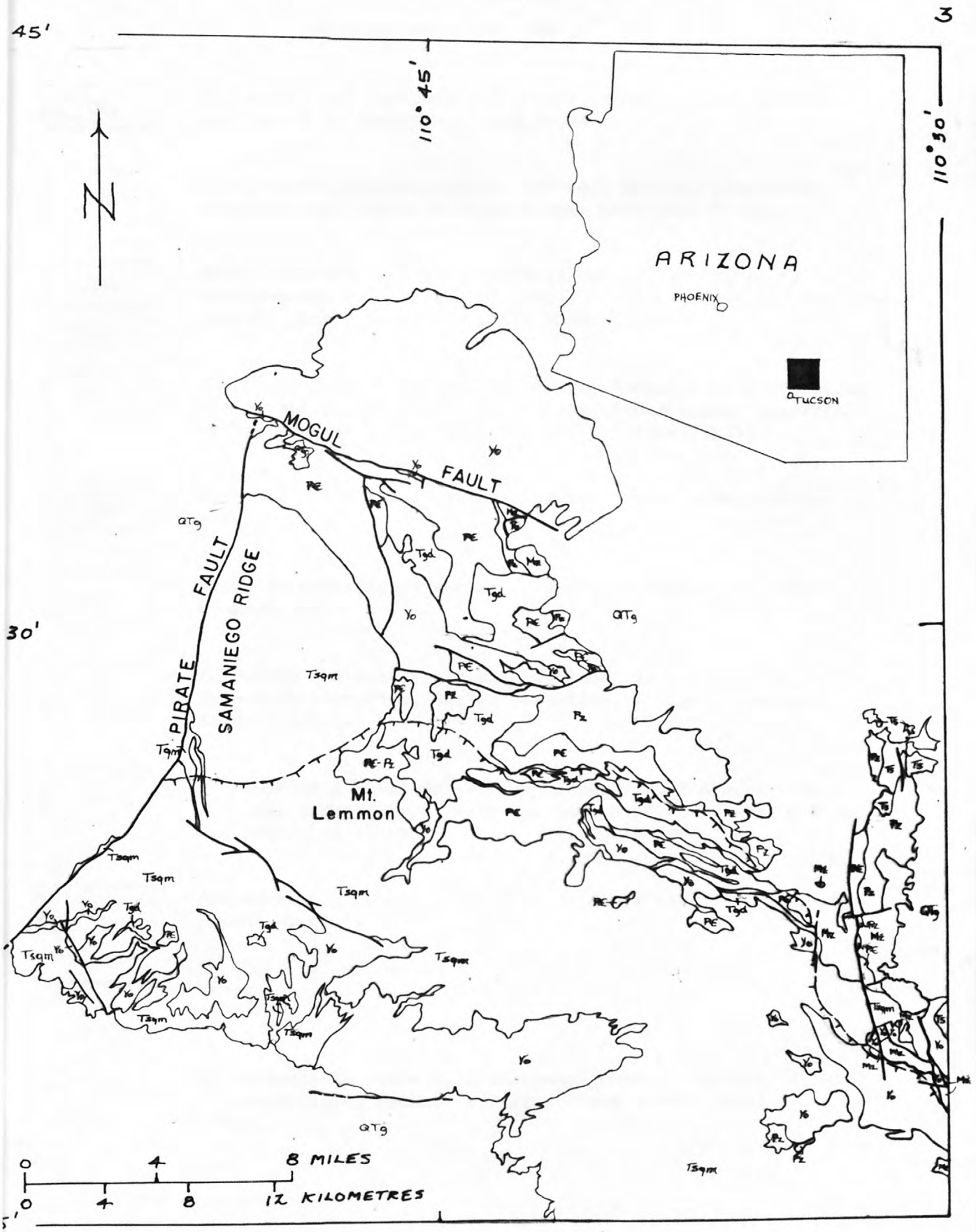

Figure 1.--Geologic sketch map of the Santa Catalina Mountains.

EXPLANATION FOR FIGURE 1

QTg	Quaternary and Tertiary sedimentary rocks: sand, gravel, conglomerate, sandstone, lake deposits
Ts	Tertiary sedimentary rocks: redbeds, shales, sandstones, conglomerates, minor volcanics near east edge of map
Tqm	Quartz monzonite of the Tortolita Mountains: fine- to medium-grained equigranular dikes. Probably correlative with similar rocks in the Tortolita Mountains
Tsqm	Quartz monzonite of Samaniego Ridge; includes porphyritic and equigranular phases and large areas with abundant xenoliths of Precambrian Y Oracle Granite of Peterson (1938)
Tgd	Quartz diorite (Leatherwood), granodiorite, granodiorite porphyry
Mz	Mesozoic sedimentary rocks: limestone, sandstone, shale, conglomerate
Pz	Paleozoic sedimentary rocks: includes Naco Limestone, Escabrosa Limestone, Martin Formation, Abrigo Formation, Bolsa Quartzite
P€	Precambrian X Pinal Schist and Precambrian Y Apache Group: Includes areas (P€-Pz) near Mt. Lemmon of mixed Apache Group and Paleozoic rocks
Yo	Precambrian Y Oracle Granite of Peterson (1938): older than Apache Group
———	Fault
⊤ ⊤ ⊤ ⊤	Approximate location of gradational contact between foliated and nonfoliated rocks. Foliated rocks on the side with the barbs.

of the batholith is gradational. The approximate location on the contact is shown on figure 1.

The fabric of the northward-extending mass of the batholith east of the Pirate fault and north of the gneissic front near Cargadero Canyon is typically igneous: the rock is massive except for joints and sparse aplite dikes. Textures are porphyritic with a medium-grained hypidiomorphic groundmass, and locally near the northeastern margin of the batholith equigranular hypidiomorphic granular. In this part of the batholith, penetrative deformation and rock alteration are absent, suggesting no subsolidus reheating. Because the minerals dated are unchanged since crystallization, our radiometric ages from this area (table 1 and fig. 2) are the prime basis for our interpretation of the age of crystallization and the cooling history of the batholith.

In contrast, the rocks forming the gneissic parts of the batholith show strong cataclasis and mylonitization, and in the foliation planes, secondary muscovite and some secondary biotite abounds; primary biotite may also have been rotated into the movement planes. The rock is metamorphic, the deformation penetrative, and the rock types are gneisses and schists.

The distribution of the gneissic and nongneissic parts of the batholith is locally erratic. Although most of the batholith shown on figure 1 is gneissic, patches of relatively massive quartz monzonite occur within the gneissic area, particularly in the southeast part of the area of figure 1. Some of the deformation extends as much as 3 km beyond the limits of the batholith. The sedimentary rocks adjacent to the batholith along the northern flank of the mountains have been so intensely sheared and recrystallized that the original formations generally cannot be distinguished from one another. Here, too, the contact between sheared and unsheared sedimentary rocks is gradational. In the nongneissic terrane, comparatively few aplite and pegmatite dikes occur. In the gneissic terrane, however, both the intrusive and country rocks contain locally abundant pegmatite dikes, some of which are foliated, but others are massive.

RADIOMETRIC AGES

Potassium-argon and fission-track ages (tables 1 and 2) of unaltered and undeformed minerals from the quartz monzonite of Samaniego Ridge indicate an apparent middle Tertiary age of crystallization of the batholith; they also give some information on the cooling history. The age of deformation is more ambiguous. Our new ages, which are from one biotite-muscovite mineral pair derived from deformed quartz monzonite, suggest deformation followed crystallization of the quartz monzonite so closely that no age difference is discernible between gneissic and nongneissic phases (table 1). However, the published K-Ar

Table 1.--*New fission-track and K-Ar ages of the quartz monzonite of Samaniego Ridge and the quartz monzonite of the Tortolita Mountains, from the Santa Catalina and Tortolita Mountains*

[Analysts: S. C. Creasey, K-Ar; R. A. Ashley, fission track]

Loc. fig.	Sample no.	Mineral dated	Method	Apparent age	Rock type	Location	Comments
II	GGN-S1	Biotite	K-Ar	22.7±0.7	Quartz monzonite of Samaniego Ridge	32°22' N. 110°43' W.	Gneissic
		Muscovite	K-Ar	24.1±0.7			
		Apatite	F.T.	18.7±2.7			
IV	ML-61	Biotite	K-Ar	24.0±0.7	Quartz monzonite of Samaniego Ridge	32°27.5' N. 110°52' W.	Massive, porphyritic with medium-grained hypidiomorphic granular groundmass
		Hornblende	K-Ar	22.3±0.7			
		Apatite	F.T.	20.2±2.1			
		Zircon	F.T.	26.3±3.4			
		Sphene	F.T.	27.5±3.1			
IV	ML-60	Biotite	K-Ar	23.5±0.7	Mafic inclusion	32°27.5' N. 110°53' W.	Original rock formation is uncertain
		Hornblende	K-Ar	36.1±1.0			
		Apatite	F.T.	20.7±2.5			
		Sphene	F.T.	27.9±3.7			
VII	BR-21	Biotite	K-Ar	23.1±0.7	Quartz monzonite of Samaniego Ridge	31°31.5' N. 110°50' W.	Massive, porphyritic with medium-grained hypidiomorphic granular groundmass
		Hornblende	K-Ar	23.4±1.2			
		Apatite	F.T.	22.8±2.8			
		Zircon	F.T.	28.1±3.3			
		Sphene	F.T.	29.1±3.0			
VIII	BR-16	Biotite	K-Ar	23.2±0.7	Quartz monzonite of Samaniego Ridge	32°31.5' N. 110°48' W.	Massive, medium-grained hypidiomorphic granular
		Apatite	F.T.	19.8±2.1			
		Zircon	F.T.	25.1±2.5			
		Sphene	F.T.	27.2±3.1			
---	RC3-1	Biotite	K-Ar	20.6±0.6	Quartz monzonite of Samaniego Ridge	32°29.5' N. 111°04' W.	Ages probably reset by gneissic dikes of quartz monzonite of Tortolita Mountains Location not on figure 4. Sample from Tortolita Mountains
		Hornblende	K-Ar	21.1±0.6			
---	RC-25	Biotite	K-Ar	22.1±0.7	Quartz monzonite of Tortolita Mountains	32°28' N. 111°02' W.	Sample from Tortolita Mountains Location not on figure 4
		Apatite	F.T.	18.0±2.4			
VI	ML-105	Apatite	F.T.	16.5±2.1	Quartz monzonite of Tortolita Mountains	32°27.5" N. 110°58' W.	Massive, slight foliation, fine-grained hypidiomorphic granular

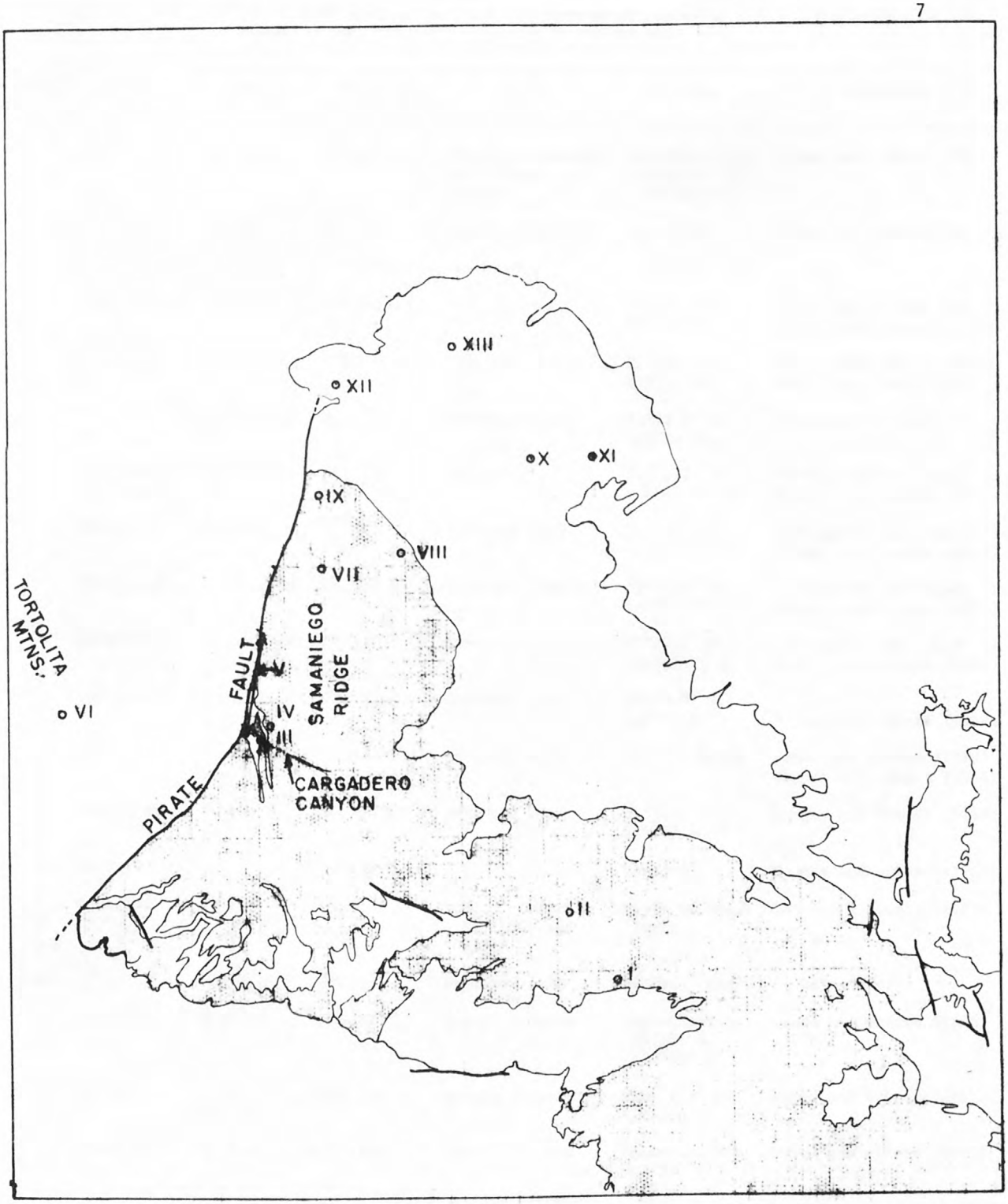

Figure 2.--Locations of samples listed in tables 1, 2, and 3. Stipple pattern indicates the outcrop area of the quartz monzonite of Samaniego Ridge.

Table 2.--*Previously published K-Ar ages of the quartz monzonite of Samaniego Ridge, Oracle Granite, and gneissic rocks, Santa Catalina and Tortolita Mountains*

Location, figure	Sample no.	Mineral dated	Apparent age (m.y.)	Rock type	Location	Reference
III	PED-16-59	Biotite	25.0±3	Quartz monzonite of Samaniego Ridge	Approximately 32°26.5' N. 110°52.2' W.	Damon and others (1963)
III	PED-17-59	Biotite	24.0±3	Quartz monzonite of Tortolita Mountains[1]	Approximately 32°26.5' N. 110°52.2' W.	Damon and others (1963)
II	PED-4a-58	Biotite	24.8±1.0	Gneissic rock	32°22.1' N. 110°43' W.	Damon and others (1963) Mauger and others (1968)
II	PED-4a-58	Muscovite	29.5±0.9	Gneissic rock	32°22.1' N. 110°43' W.	Mauger and others (1968) Damon and others (1963)
II		Muscovite	32 ±3	Gneissic rock	32°22.1' N. 110°43' W.	Catanzaro and Kulp (1964)
I	PED-18-62L	Muscovite	25.4±1	Gneissic rock	32°20.3' N. 110°41.4' W.	Livingston and others (1967) Mauger and others (1968)
I	PED-18-62L	Biotite	25.1±1.0	Gneissic rock	32°20.3' N. 110°41.4' W.	Livingston and others (1967) Mauger and others (1968)
I	PED-18-62L	Orthoclase	26.8±0.8	Gneissic rock	32°20.3' N. 110°41.4' W.	Livingston and others (1967) Mauger and others (1968)
I	PED-18-62L	Plagioclase	[2]29.3±1.0	Gneissic rock	32°20.3' N. 110°41.4' W.	Livingston and others (1967) Mauger and others (1968)
I	PED-18-62D	Biotite	27.5±0.9	Gneissic rock	32°20.3' N. 110°41.4' W.	Mauger and others (1968)
Uncertain	PED-4-58	Muscovite	25.9±1.1	Gneissic rock	Sabino Canyon	Damon and others (1963) Mauger and others (1968)
I	PED-56-66	Muscovite	31.2±0.9	Gneissic rock	32°20.6' N. 110°55.4' W.	Mauger and others (1968)
Uncertain	RM-1-66	Muscovite	31.2±0.9		Unknown	Mauger and others (1968)
IX	PED-27-57	Biotite	38.5±3	Quartz monzonite of Samaniego Ridge	South of Mogul fault	Damon and others (1963)
Uncertain		Whole rock	20.5±3	Trachyte dike	Ventana Canyon	Shakel (1974)
XII	PED-1-58	Biotite	49.2±3	Oracle Granite	Approximately 32°35' N. 110°50' W.	Damon and others (1963)
XIII	PED-3-58	Pegmatite Muscovite	1420 ±40	Oracle Granite	Near Oracle, Arizona	Damon and others (1963)
XI	PED-2-58	Biotite	1420 ±40	Oracle Granite	Approximately 32°33' N. 110°43' W.	Damon and others (1963)
	PED-20-62	Biotite	27.3±0.9	Gneissic rock	32°28.8' N. 111°05' W.	Mauger and others (1968)

[1]Described as a fine-grained granite. Probably the quartz monzonite of the Tortolita Mountains, but could be a younger aplite.

[2]Livingston and others (1967) and Mauger and others (1968) believe this figure does not indicate the age of the rock.

ages, which were obtained from 10 samples of either biotite or muscovite from three localities in foliated rock (table 2), are discernibly older than the age of crystallization; this age difference will be discussed later.

K-Ar isotopic ages from biotite and hornblende, samples ML-61 and BR-21, and from biotite, samples ML-60 and BR-16, are concordant; the range, including the ranges of analytical uncertainty for all the individual ages, is from 21.6 to 24.7 m.y., the mean is 23.3 m.y., and the middle point of the range is 23.2 m.y. Biotite from sample PED-16-59 (table 2) is essentially the same (25.0±3 m.y.) considering the larger stated analytical error.

Concordant ages of two biotite-hornblende mineral pairs and the concordance between the two pairs, which are from different localities (samples ML-61 and BR-21), strongly indicate the age of crystallization. Biotite and hornblende have different argon retention properties, and it is highly unlikely that their ages would agree if the rock had been reheated subsequent to crystallization, unless the heating was so severe that all radiogenic argon was dispelled from both minerals. Such reheating, however, would leave other manifestations of alteration, which are not present.

Hornblende from sample ML-60 (table 1) has a K-Ar age of 36.1±1 m.y. It is one of a mineral pair of which the other is biotite with a K-Ar age of 23.5±0.7 m.y. Sample ML-60 is a mafic inclusion in the quartz monzonite of Samaniego Ridge. Because the biotite age agrees with several other K-Ar ages, including mineral pairs, we hold that it has been completely equilibrated to the age of the quartz monzonite host. We do not know whether the older age of the hornblende is due to excess argon from a local abnormally high, partial pressure of argon in the quartz monzonite, or whether it is due to partial retention of the radiogenic argon that was generated in the rock prior to intrusion of the batholith and prior to the thermal metamorphism of the inclusion by the quartz monzonite magma.

The quartz monzonite of the Tortolita Mountains is the equigranular younger phase of the composite batholith. It intrudes the porphyritic quartz monzonite of Samaniego Ridge in the Tortolita Mountains, and dikes of the equigranular phase cut the porphyritic Samaniego in Cargadero Canyon in the Santa Catalina Mountains. Two K-Ar biotite ages of the quartz monzonite of the Tortolita Mountains, as given by sample RC-25 (table 1) and perhaps by sample PED-17-59 (table 2) are 22.1±0.7 and 24.0±3 m.y., respectively. The range in age of the two samples overlap in part, and until more ages are determined, our best estimate of the age of the quartz monzonite is between 21 and 25 m.y. Rock sample RC-3-1, which is gneissic porphyritic quartz monzonite of Samaniego Ridge, was collected within 1 metre of dikes of the equigranular younger

phase of the batholith. A biotite-hornblende mineral pair (sample RC-3-1, table 1) from this rock sample gives K-Ar age of 20.6±0.6 and 21.1±0.6 m.y., respectively. We believe (1) that these ages were reset by the heat of the dikes and therefore reflect the age of the quartz monzonite of the Tortolita Mountains, and (2) that the quartz monzonite of the Tortolita Mountains, although a part of the composite batholith, is perceptibly younger than the quartz monzonite of Samaniego Ridge, using the K-Ar dating technique. The fission-track ages on apatite (samples RC-25 and ML-105, table 1), which will be discussed later, support this contention.

The new K-Ar ages of metamorphic biotite and muscovite (sample GGN-S1, table 1) from the gneissic quartz monzonite of Samaniego Ridge are 22.7±0.7 and 24.1±0.7 m.y., respectively. Their average age (23.4 m.y.) and range (22.0-24.8) are essentially the same as the average age and range for igneous biotite and hornblende from the massive quartz monzonite. These ages, however, differ from the previously published ages of metamorphic biotites and muscovites, which range from 23.8 to 35 m.y., including analytical error ranges for lowest and highest ages; their average age is 27.6 m.y. (gneissic rocks of table 2). We have no adequate explanation for the difference between our ages and the previously published ages. A possible explanation might be related to the proximity of some of the earlier sampled gneisses to outcrops of Oracle Granite (locality I, fig. 2). This, however, could not explain the age differences of the samples collected at locality II. Within the ages previously published of micas from gneissic rocks, the average age of the four biotites is 26.1 m.y. and of the five muscovites is 28.8 m.y. We also have no data to explain this difference, but Mauger, Damon, and Livingston (1968, p. 586) believe that the older age of the muscovite is due to excess inherited argon trapped in large grains. Among the dated muscovite samples, the coarser the grain size, the older the apparent age.

The fission-track ages (table 1) are internally consistent, and suggest that the batholith cooled slowly over a relatively long period of time. From annealing studies (Fleischer and others, 1965; Naeser and Faul, 1969; Calk and Naeser, 1973; Naeser, 1976), which indicate the temperatures at which the minerals begin to accumulate tracks, apatite should indicate the youngest age followed by zircon and sphene. For the massive quartz monzonite of Samaniego Ridge, the average age and the range, including analytical error, for apatite is 20.9 and 17.7-25.6 m.y., for zircon 26.5 and 22.6-31.4 m.y., and for sphene 27.9 and 24.1-32.1 m.y. (table 1 and fig. 2). As an approximation, the cooling history of the samples should reflect that of the batholith, and on this basis, these ages suggest that the batholith had cooled to about 500°C about 28 m.y. ago and had reached about 100°C about 21 m.y. ago. The average age of 26.5 m.y. for zircons suggests that zircon began to accumulate tracks at a somewhat lower temperature than sphene. The

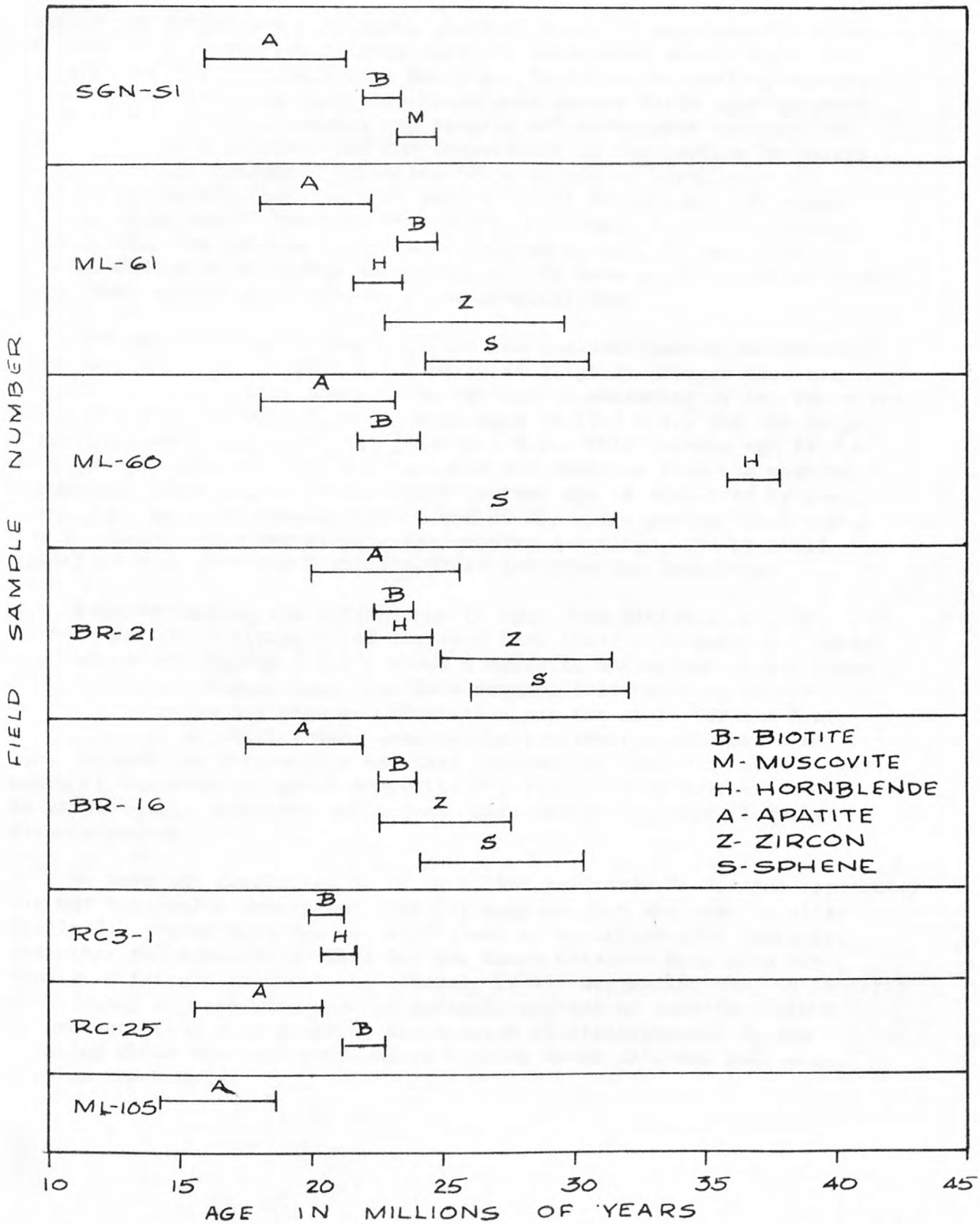

Figure 3.--Bar graphs of new fission-track and K-Ar ages of the quartz monzonite Samaniego Ridge and the quartz monzonite of the Tortolita Mountains, Santa Catalina and Tortolita Mountains.

biotite and hornblende K-Ar ages, however, indicate more rapid cooling. If there is a protracted cooling history, hornblende should begin to collect radiogenic argon before biotite. To judge the cooling history from the fission-track ages, the hornblende should yield ages slightly older than biotite. Actually the biotite and hornblende indicate the same ages, which implies that the temperature of the cooling batholith dropped through the argon retention temperatures of hornblende and biotite so rapidly that the K-Ar method cannot detect any difference between their ages. The data from the two techniques, taken together, suggest that the cooling and crystallization history is more complex than is indicated by either method alone. We have no data, on the other hand, that allows us to delineate the complexities.

The apatite fission-track age for the gneissic quartz monzonite of Samaniego Ridge is 18.7±2.7 m.y., which is slightly younger than the average for the massive phase. For the quartz monzonite of the Tortolita Mountains, the average of two apatite ages is 17.3 m.y., and the range, including analytical error, is 14.4-20.4 m.y. This average age is 3.6 m.y. younger than the 20.9 average ages for apatites from the massive porphyritic Samaniego. This younger average age is supported by the three K-Ar ages for samples RC-3-1 and RC-25, which average 21.3 m.y., 2 m.y. younger than the average for massive Samaniego, and by field relations that show the Tortolita phase intrudes the Samaniego.

Notwithstanding the differences in ages from different dating methods and the differences of our ages from those previously published, examination of figures 3 and 4 shows a magmatic and deformational event occurred about 25 m.y. ago. Our data suggest that the time interval between plutonism and intense deformation was too short for the K-Ar dating method to distinguish, whereas the previously published K-Ar ages suggest the deformation may have followed plutonism by about 4 m.y. based on the average age of muscovite and biotite from gneissic rocks. In either case, plutonism and intense deformation are significantly close together.

We have not determined Rb-Sr ages, but published Rb-Sr ages apparently are not internally consistent even for samples from the same locality (table 3). These data are not sufficient to be interpreted properly, and other published Rb-Sr data for the Santa Catalina Mountains are equally difficult to interpret (Shakel, 1974), suggesting that an in-depth Rb-Sr study coupled with careful geologic control of sampling, might be prudent prior to attempting explanation of discrepancies in the existing Rb-Sr data and differences between Rb-Sr data and K-Ar and fission-track data.

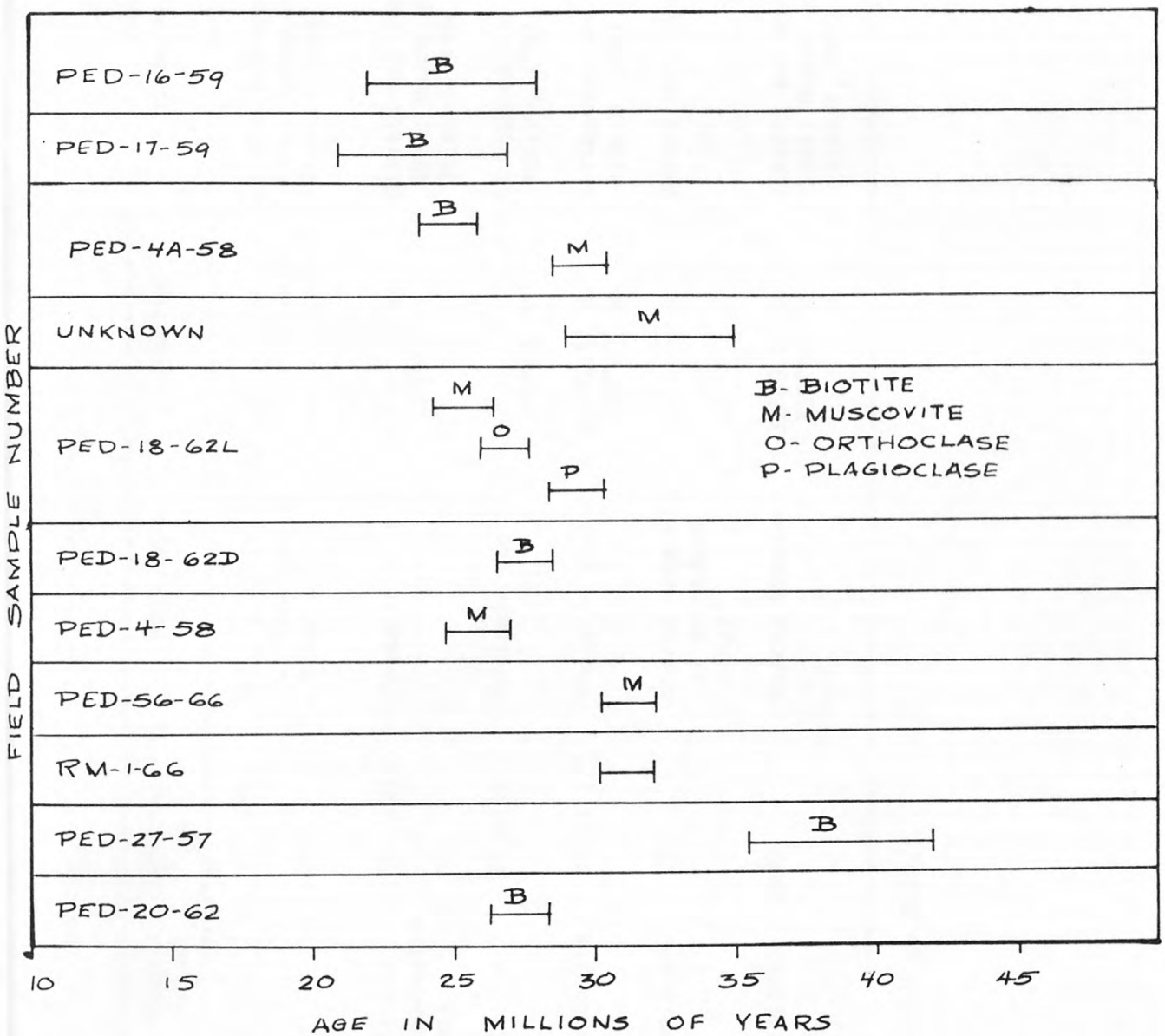

Figure 4.--Bar graphs of published K-Ar ages of quartz monzonite of Samaniego Ridge and gneissic rocks, Santa Catalina and Tortolita Mountains.

Table 3.--*Previously published Rb-Sr ages of the quartz monzonite of Samaniego Ridge, Oracle Granite, and gneissic rocks, Santa Catalina Mountains*

Location figure	Sample no.	Mineral dated	Apparent age m.y.	Rock type	Location	Reference
VI	---	Biotite	30. ±30	Quartz monzonite of Samaniego Ridge	500 ft from Pirate fault east of Canada Del Oro	Giletti and Damon, 1961; Damon and Giletti, 1961
II	---	Biotite muscovite mix	150. ±90	Gneissic rock	32°22.1' N. 110°43' W.	Giletti and Damon, 1961; Damon and Giletti, 1961
II	PED-4A-58	Biotite	23.9±14	Gneissic rock	32°22.1' N. 110°43' W.	Livingston and others, 1967
II	PED-4A-58	Muscovite	37.6± 1.0	Gneissic rock	32°22.1' N. 110°43' W.	Livingston and others, 1967
VI		Whole rock	90	Quartz monzonite of Samaniego Ridge[1]	---	Shakel and others, 1972
XI		Biotite	1450	Oracle Granite	32°33.5' N. 110°44' N.	Giletti and Damon, 1961; Damon and Giletti, 1961

[1]Called "Catalina granite" by Shakel.

EPILOGUE

Special mention of some of the ideas of B. N. Moore and C. F. Tolman, Jr., and their colleagues is merited because of their extensive and careful work. The short summary report (Moore and others, 1949) mentions the quartz monzonite of Samaniego Ridge (Santa Catalina granitic complex) only briefly, and it scarcely mentions the deformation responsible for the gneisses. It does indicate, however, that the pluton was of batholithic size; therefore, although this concept was available in 1949, it subsequently seems to have had little acceptance.

The following excerpts from B. N. Moore and others (unpub. data, 1938, 321 p.) clearly reveal that their concepts on the extent and origin of the batholith and on the relationships of deformation to the batholith differ little from ours. Their Late Cretaceous or early Tertiary age for the pluton was based on field relations with which we concur, and our middle Tertiary designation is based on radiometric ages obtained only recently.

> "For convenience the granites in the Tortollita (sic) Mountains, Mt. Lemmon, Youtcy Ranch, and Happy Valley are described separately in this report but they are considered parts of the Catalina batholith and on the map the symbol of the Catalina granite is applied to all these localities.
>
> "It may be suggested that the post-Cretaceous igneous rocks were intruded during a period of stresses which reached their peak in the intrusion of the granites of the Catalina batholith. Whether this zone can be traced east and west from this region and whether other regions of Tertiary thrusting show evidence of earlier deformation remains to be shown.
>
> "These intrusions are of great interest in the history of this region because they differ from those to the north and to the south. The alignment of the bodies and the presence of strong pressure effects in the formation of the gneisses suggest intrusion along a zone of deformation. The great amounts of solutions probably resulted from the effects of pressure in squeezing out solutions from partly consolidated magmas."

REFERENCES CITED

Banks, N. L., 1976, Reconnaissance geologic map of the Mount Lemmon quadrangle, Arizona: U.S. Geol. Survey Misc. Field Studies Map MF-747. (In press)

Calk, L. C., and Naeser, C. W., 1973, The thermal effect of a basalt intrusion of fission tracks in quartz monzonite: Jour. Geology, v. 81, p. 189-198.

Catanzaro, E. J., and Kulp, J. L., 1964, Discordant zircons from the Little Belt (Montana), Beartooth (Montana), and Santa Catalina (Arizona) Mountains: Geochim. et Cosmochim. Acta, v. 28, p. 87-124.

Creasey, S. C., and Theodore, T. G., 1975, Preliminary reconnaissance geologic map of the Bellota Ranch quadrangle, Pima County, Arizona: U.S. Geol. Survey Open-file Rept. 75-295.

Damon, P. E., Erickson, R. C., and Livingston, D. E., 1963, K-Ar dating of Basin and Range uplift Catalina Mountains, Arizona: Natl. Acad. Sci.--Natl. Research Council Pub. 1075, p. 113-121.

Damon, P. E., and Giletti, B. J., 1961, The age of the basement rocks of the Colorado Plateau and adjacent areas, in Geochronology of rock systems: New York Acad. Sci. Annals, v. 91, art. 2, p. 443-453.

Fleischer, R. L., Price, P. B., and Walker, R. M., 1965, Effects of temperature, pressure, and ionization on the formation and stability of fission tracks in minerals and glasses: Jour. Geophys. Research, v. 70, p. 1497-1502.

Giletti, B. J., and Damon, P. E., 1961, Rubidium-strontium ages of some basement rocks from Arizona and northwestern Mexico: Geol. Soc. America Bull., v. 72, no. 4, p. 639-643.

Livingston, D. E., Damon, P. E., Mauger, R. L., Bennett, Richmond, and Laughlin, A. W., 1967, Argon 40 in cogenetic feldspar-mica mineral assemblages: Jour. Geophys. Research, v. 72, no. 4, p. 1361-1375.

Mauger, R. L., Damon, P. E., and Livingston, D. E., 1968, Cenozoic argon ages from metamorphic rocks from the Basin and Range province: Am. Jour. Sci., v. 266, no. 7, p. 579-589.

Moore, B. N., Tolman, C. F., Jr., Butler, B. S., and Hernon, R. M., 1949, Geology of the Tucson quadrangle, Arizona: U.S. Geol. Survey open-file report, 20 p.

Naeser, C. W., 1976, Fission track dating: U.S. Geol. Survey Open-file Rept. 76-190.

Naeser, C. W., and Faul, H. O., 1969, Fission-track annealing in apatite and sphene: Jour. Geophys. Research, v. 74, no. 2, p. 705-710.

Peterson, N. P., 1938, Geology and ore deposits of the Mammoth mining camp area, Pinal County, Arizona: Arizona Bur. Mines Bull. 144, Geol. ser. 11, 63 p.

Shakel, D. W., 1974, The geology of layered gneisses in part of the Santa Catalina forerange, Pima County, Arizona: Arizona Univ., Tucson, M.S. thesis, 233 p.

Shakel, D. W., Livingston, D. E., and Pushkar, P. D., 1972, Geochronology of crystalline rocks in the Santa Catalina Mountains, near Tucson, Arizona: Geol. Soc. America, Abs. with Programs, v. 4, p. 408.

Shapiro, Leonard, 1975, Rapid analyses of silicates, carbonate, and phosphate rocks, revised ed.: U.S. Geol. Survey Bull. 1401, 76 p.

Table 4.--*Chemical, spectrographic, normative, and modal analyses of rocks from the Santa Catalina and Tortolita Mountains*

[Rapid rock analyses: analyst Hezekiah Smith, analytical method as described under "single solution" by Shapiro (1975). Analysis of Cl by R. Moore and B. McCall; spectrophotometric analytical method. Quantitative spectrographic analyses: analyst Chris Heropoulos. The results are reported to have significant figures and have an overall accuracy near the limit of detection where only one digit is intended]

	Massive quartz monzonite of Samaniego Ridge			Gneissic quartz monzonite of Samaniego Ridge	Quartz monzonite of Tortolita Mountains	Gneissic Oracle Granite
Rapid rock analyses						
Lab. no.	M124370WD	M124371WD	M124372WD	M124757WD	M124374WD	M124373WD
Field no.	BR-16	BR-21	ML-61	GGN-S1	ML-105	ML-62R
SiO_2	73.2	68.6	67.0	74.1	73.2	70.0
Al_2O_3	13.6	15.3	15.5	15.1	14.4	15.4
Fe_2O_3	.89	1.3	2.0	.33	.72	1.6
FeO	.64	1.3	1.9	.52	.52	.92
MgO	.50	.90	1.7	.08	.24	.52
CaO	1.1	2.2	3.0	1.3	1.1	1.9
Na_2O	3.6	3.8	4.2	4.3	3.5	3.4
K_2O	4.6	4.6	3.8	3.9	5.0	4.8
H_2O+	.32	.79	.72	.49	.42	.74
H_2O-	.22	.19	.08	.05	.17	.26
TiO_2	.20	.38	.62	.01	.10	.34
P_2O_5	.11	.19	.28	.04	.07	.20
MnO	.03	.05	.09	.02	.02	.04
CO_2	.02	.01	.02	.02	.02	.01
Cl	.01	.01	.005	.01	.003	.005
F	.03	.01	.06	<.01	<.01	<.01
Sum	99+	100-	101-	100+	99+	100+
Quantitative spectrographic analyses						
Plate no. EM-1224						
Ti %	0.15	0.27	0.37	0.05	0.11	0.30
Mn (ppm)	370	470	800	260	250	330
Ba	330	1100	640	1500	1100	2400
Be	7	5	6	N1	2	N1
Co	N2	8	11	N2	N2	8
Cr	N2	8	12	N2	N2	N2
Cu	13	9	9	11	5	65
Ni	1.6	8	14	N1	1.5	2
Sc	N1.5	7	8	N1.5	N1.5	7
Sr	170	350	380	220	180	650
V	23	44	72	N3	16	39
Y	10	19	26	N10	10	26
Zr	48	36	110	31	82	50
Ga	18	18	21	12	16	17
Yb	1	1	2	N1	1	1
Norms						
Quartz	32.2	23.2	19.5	31.0	31.4	27.6
corundum	1.0	.6	---	1.6	1.5	1.7
orthoclase	27.5	27.3	22.3	23.0	29.8	28.4
albite	30.8	32.3	35.2	36.3	29.8	28.8
anorthite	4.7	9.7	12.1	6.0	4.9	8.1
wollastonite	---	---	.3	---	---	---
enstatite	1.3	2.3	4.2	.2	.6	1.3
ferrosilite	.2	.8	1.0	.7	.2	---
forsterite	---	---	---	---	---	---
fayalite	---	---	---	---	---	---
magnetite	1.3	1.9	2.9	.5	1.1	2.1
ilmenite	.4	.7	1.2	tr	.2	.6
apatite	.3	.5	.7	.1	.2	.5
Modes						
quartz	33.0	16.3	30.4	33.2	39.2	N
K-spar and perthite	38.3	30.5	24.1	22.8	31.2	o t
plagioclase	24.4	41.0	37.7	35.8	26.4	
biotite	2.9	9.1	6.1	3.8	3.2	d
hornblende	---	1.4	.3	---	---	e
magnetite	.9	1.0	.5	.2	tr	t
sphene	.3	.3	.6	tr	---	e
apatite	.2	.4	.3	tr	tr	r
zircon	tr	tr	tr	tr	tr	m
muscovite	---	---	---	4.2	---	i
garnet	---	---	---	tr	---	n
Sum	100	100	100	100	100	e d
An-content of plagioclase	An_{20}?	An_{20}	An_{20}	An_{20}	An_{20}	. An_{20}?

N = not detected at value shown.

Analytical data for fission-track ages for Santa Catalina and Tortolita Mountains

[Methods for fission-track age determinations are similar to those currently employed by C. W. Naeser (Naeser, 1976); $\lambda_F = 6.85 \times 10^{-17}$ yr^{-1}. Numbers of tracks counted are given in parentheses. The ± figures for estimated analytical uncertainty are based on numbers of tracks counted for ρs, ρi, and ϕ determinations]

Sample	Mineral	ρsx10^6, tracks/cm^2	ρix10^6, tracks/cm^2	ϕx10^{15}, neutrons/cm^2	Age ± 2σ x10^6 years
ML-61	Apatite	0.323 (1220)	3.50 (1487)	3.59	20.2±2.1
ML-61	Zircon	3.29 (625)	14.9 (1330)	1.83	26.3±3.4
ML-61	Sphene	1.15 (1014)	4.74 (2087)	1.85	27.5±3.1
BR-21	Apatite	0.204 (773)	1.97 (835)	3.59	22.8±2.8
BR-21	Zircon	5.18 (797)	18.1 (1396)	1.61	28.1±3.3
BR-21	Sphene	2.79 (1308)	9.54 (2238)	1.63	29.1±3.0
ML-60	Apatite	.201 (761)	2.13 (905)	3.59	20.7±2.5
ML-60	Sphene	.918 (551)	3.76 (1129)	1.87	27.9±3.7
BR-16	Apatite	.305 (1152)	3.38 (1434)	3.59	19.8±2.1
BR-16	Zircon	4.98 (1436)	19.7 (2841)	1.62	25.1±1.5
BR-16	Sphene	1.39 (912)	5.15 (1691)	1.65	27.2±3.1
Ggn-S1	Apatite	.0393 (297)	.462 (1749)	3.59	18.7±2.7
RC-25	Apatite	.113 (429)	1.23 (2066)	3.19	18.0±2.4
ML-105	Apatite	.163 (617)	2.17 (921)	3.59	16.5±2.1

Analytical data for K-Ar ages for the Santa Catalina and Tortolita Mountains

Sample	Mineral	Percent	K_2O	$*Ar^{40}$moles/gm	$*Ar^{40}/\Sigma Ar^{40}$	Age, 10^6 yrs.
GGN-S1	Biotite	8.79	8.78	2.96482×10^{-10}	62.2%	22.7±0.7
GGN-S1	Muscovite	9.78	9.75	3.50169×10^{-10}	74.6	24.1±0.7
ML-61	Biotite	8.59	8.62	3.07432×10^{-11}	78.6	24.0±0.7
ML-61	Hornblende	.927	.924	3.07276×10^{-10}	38.6	22.3±0.7
ML-60	Biotite	9.10	9.10	3.18397×10^{-10}	78.4	23.5±0.7
ML-60	Hornblende	1.042	1.040	5.70900×10^{-11}	53.0	36.8±1.0
BR-21	Biotite	7.28	7.32	2.50623×10^{-10}	63.8	23.1±0.7
BR-21	Hornblende	.598	.598	2.07901×10^{-11}	20.4	23.4±1.2
BR-16	Biotite	9.10	9.10	3.13143×10^{-10}	67.3	23.2±0.2
RC3-1	Biotite	8.64	8.63	2.64175×10^{-10}	52.5	20.6±0.6
RC3-1	Hornblende	.933	.934	2.92466×10^{-11}	49.9	21.1±0.6
RC-25	Biotite	8.33	8.40	2.74315×10^{-10}	69.1	22.1±0.7

$\lambda_\varepsilon = 0.585 \times 10^{-10}$/yr.

$\lambda_\beta = 4.72 \times 10^{-10}$/yr.

$K^{40}/K_{total} = 1.19 \times 10^{-4}$ mole/mole